ADVANCED MATERIALS
www.advmat.de

Electrical Conductivity, Selective Adhesion, and Biocompatibility in Bacteria-Inspired Peptide–Metal Self-Supporting Nanocomposites

*Tom Guterman, Nicole L. Ing, Sharon Fleischer, Pavel Rehak, Vasantha Basavalingappa, Yamanappa Hunashal, Ramachandra Dongre, Srinivasarao Raghothama, Petr Král, Tal Dvir, Allon I. Hochbaum, and Ehud Gazit**

Bacterial type IV pili (T4P) are polymeric protein nanofibers that have diverse biological roles. Their unique physicochemical properties mark them as a candidate biomaterial for various applications, yet difficulties in producing native T4P hinder their utilization. Recent effort to mimic the T4P of the metal-reducing *Geobacter sulfurreducens* bacterium led to the design of synthetic peptide building blocks, which self-assemble into T4P-like nanofibers. Here, it is reported that the T4P-like peptide nanofibers efficiently bind metal oxide particles and reduce Au ions analogously to their native counterparts, and thus give rise to versatile and multifunctional peptide–metal nanocomposites. Focusing on the interaction with Au ions, a combination of experimental and computational methods provides mechanistic insight into the formation of an exceptionally dense Au nanoparticle (AuNP) decoration of the nanofibers. Characterization of the thus-formed peptide–AuNPs nanocomposite reveals enhanced thermal stability, electrical conductivity from the single-fiber level up, and substrate-selective adhesion. Exploring its potential applications, it is demonstrated that the peptide–AuNPs nanocomposite can act as a reusable catalytic coating or form self-supporting immersible films of desired shapes. The films scaffold the assembly of cardiac cells into synchronized patches, and present static charge detection capabilities at the macroscale. The study presents a novel T4P-inspired biometallic material.

Bacterial type IV pili (T4P) are an abundant class of supramolecular nanofibers composed mainly of pilin protein monomers.[1] In the metal-reducing *Geobacter sulfurreducens* (GS), T4P participate in anaerobic respiration by facilitating physical contact with and subsequent electron transfer to extracellular metal species, such as Fe(III)-oxide-containing minerals[2] and U ions.[3] The molecular underpinnings of this interaction are unknown, as is the exact structure of the GS T4P,[4] yet evidence suggests that the physical contact is mediated by the evolutionary variable polar C-terminal region of the GS pilin monomer.[5] This is in line with the fact that the C-terminal region of homologous pilins is solvent-exposed to interact with the molecular environment, whereas the N-terminal region is associated with pilin in vivo assembly and constitutes the hydrophobic core of the assembled pilus.[6]

In light of the unique biological functionality of GS T4P, we envision their

T. Guterman, Dr. S. Fleischer, Dr. V. Basavalingappa, Prof. T. Dvir, Prof. E. Gazit
Department of Molecular Microbiology and Biotechnology
George S. Wise Faculty of Life Sciences
Tel Aviv University
Tel Aviv 6997801, Israel
E-mail: ehudg@post.tau.ac.il

T. Guterman, Dr. S. Fleischer, Dr. V. Basavalingappa, Prof. T. Dvir, Prof. E. Gazit
The Center for Nanoscience and Nanotechnology
Tel Aviv University
Tel Aviv 6997801, Israel

Dr. N. L. Ing, Prof. A. I. Hochbaum
Department of Chemical Engineering and Materials Science
University of California, Irvine
Irvine, CA 92697, USA

P. Rehak, Prof. P. Král
Department of Chemistry
University of Illinois at Chicago
Chicago, IL 60607, USA

The ORCID identification number(s) for the author(s) of this article can be found under https://doi.org/10.1002/adma.201807285.

DOI: 10.1002/adma.201807285

Y. Hunashal, R. Dongre, Prof. S. Raghothama
NMR Research Centre
Indian Institute of Science
Bangalore 560012, India

Prof. P. Král
Department of Physics and Department of Biopharmaceutical Sciences
University of Illinois at Chicago
Chicago, IL 60607, USA

Prof. T. Dvir
Department of Materials Science and Engineering
Iby and Aladar Fleischman Faculty of Engineering, and Sagol Center for Regenerative Biotechnology
Tel Aviv University
Tel Aviv 69978, Israel

Prof. A. I. Hochbaum
Department of Chemistry
University of California, Irvine
Irvine, CA 92697, USA

Prof. E. Gazit
Department of Materials Science and Engineering
Iby and Aladar Fleischman Faculty of Engineering
Tel Aviv University
Tel Aviv 6997801, Israel

© 2019 WILEY-VCH Verlag GmbH & Co. KGaA, Weinheim

biosynthetic peptide mimetics as a useful class of bioinspired materials.[7] Recently, we reported the self-assembly of designed 20-mer peptide building blocks into T4P-like nanofibers.[8] A reductionist study of the 20-mer peptide showed that its C-terminal segment adopts a native-like helical conformation and is nonessential for self-assembly, whereas its N-terminal segment presents a divergent β-type conformation and drives the self-assembly process.[8] While the 20-mer T4P-like nanofibers have been studied from the structural aspect, their functionality has not been explored. Due to the inherent propensity of native GS T4P to interact with metal oxide particles and metal ions, we hypothesized that an analogous interaction would occur in the case of the T4P-like peptide nanofibers. Previously, a variety of self-assembled protein[9–11] or peptide[12,13] filaments have been decorated by metals or metal oxides, and in some cases the decorated filaments were successfully utilized for specific applications.[10,11] Yet, the previously reported interactions between proteinaceous filaments and metallic species were not directly inspired by a native biological system. Moreover, substantial decoration at the single nanofilament level was typically achieved in previous studies following multistep processes or by using extrinsic additives. Here, we show that the T4P-like peptide nanofibers efficiently bind metal and nonmetal oxide particles by simple coincubation. The nanofibers also reduce ionic Au in a single-step, additive-free process that leads to their exceptionally dense decoration by gold nanoparticles (AuNPs). The thus-formed peptide–AuNPs nanocomposite presents electrical conductivity from the single-nanofiber level up and substrate-selective adhesion. Based on these properties, we show that nanocomposite coatings and self-supporting films can be easily prepared and used in chemical catalysis, static charge detection, and cardiac tissue scaffolding applications. The processes and applications explored in this work are illustrated in **Scheme 1**.

GS T4P natively interact with Fe(III) oxide. To test the peptide nanofibers for this behavior, dispersions of Fe(III) oxide nanoparticles in potassium phosphate buffer (pH 7.4, the assembly medium of the nanofibers) were incubated in the presence or absence of preformed nanofibers. While the dispersion of nanoparticles alone retained its macroscopic homogeneity during a period of 3 h, a sedimented floccule was observed in the nanofiber-supplemented (0.075 volume fraction) nanoparticle dispersion and the liquid bulk became transparent, similarly to an equivalent control dispersion of the nanofibers alone (**Figure 1**a). UV–vis spectra of the liquid bulks showed significant optical density (OD) reduction in the nanofiber-supplemented condition as compared with the nanoparticles-only control, resulting in a similar spectrum to that acquired from the nanofibers-only control (Figure 1b). Complementing transmission electron microscopy (TEM) imaging of the floccule revealed a network of nanofibers decorated with Fe(III) oxide nanoparticles (Figure 1c; pristine peptide nanofibers and oxide nanoparticles are shown in Figure S1, Supporting Information). Altogether, these data show that the peptide nanofibers bind Fe(III) oxide nanoparticles and they cosediment. Similar results were obtained when the nanoparticles were substituted with ZnO or TiO_2 nanoparticles, or with the nonmetallic SiO_2 nanoparticles and graphene oxide (GO) flakes (Figure 1; pristine oxides are shown in Figure S1,

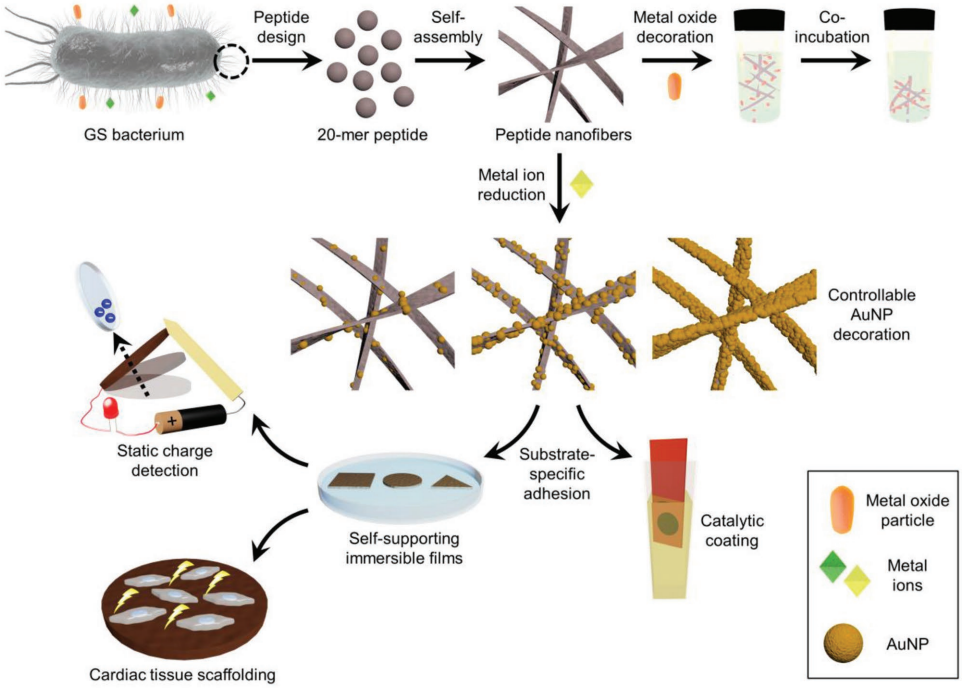

Scheme 1. Scope of the present work. Inspired by the native interaction of GS T4P with metal oxides and metal ions, analogous interaction between such species and T4P-like self-assembled peptide nanofibers was explored. Binding of metal oxides to the nanofibers, as well as the ability of the latter to reduce ionic Au, were both investigated. Peptide nanofiber–AuNPs nanocomposite was formed in a controllable manner via ionic Au reduction process by the nanofibers. Owing to its substrate-selective adhesion and electrical conductivity, the nanofiber–AuNPs nanocomposite was utilized for chemical catalysis, static charge detection, and cardiac tissue scaffolding applications.

 © 2019 WILEY-VCH Verlag GmbH & Co. KGaA, Weinheim

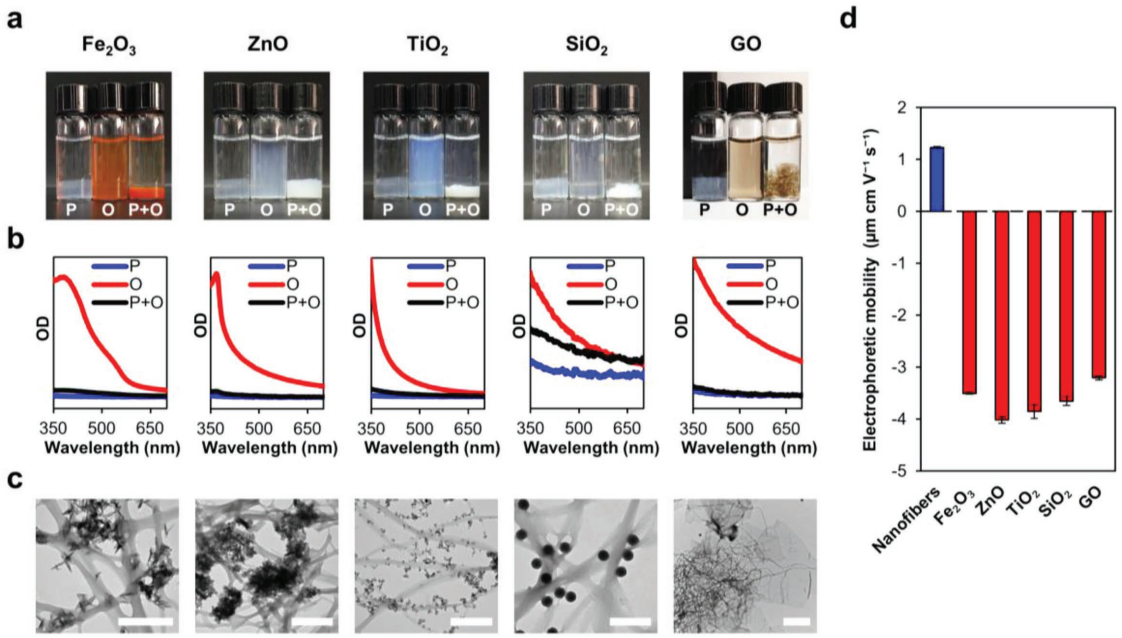

Figure 1. Binding of oxide particles to peptide nanofibers. a) Photographs of nanofiber dispersions, different dispersions of oxide particles, and peptide nanofiber-oxide mixtures. P and O denote peptide nanofibers and oxide particles, respectively. Photographs were taken following 3 h incubation. A sedimenting floccule is seen at the bottom of the vial in nanofiber dispersions and nanofiber-oxide mixtures, but not in oxide dispersions. b) UV–vis spectra of liquid bulk samples corresponding to panel (a). c) TEM images of floccule samples from the nanofibers-oxide mixtures corresponding to (a). Scale bars are 500 nm except for GO, where scale bar is 2 µm. d) Electrophoretic mobility of peptide nanofibers and oxide particles. Under the experimental conditions, attraction between opposite electrostatic charges drives the binding of oxide particles to the sedimenting peptide nanofibers. Data represent mean ± standard error of the mean ($n = 3$ samples).

Supporting Information). Hence, the nanofibers appear to present a more general ability to bind oxide materials. An electrophoretic mobility assay suggested that the binding of oxides stems from electrostatic attraction, since the oxides were negatively charged under the experimental conditions, in line with previous reports,[14] whereas the nanofibers were positively charged (Figure 1d). The peptide nanofibers therefore appear useful for the immobilization of oxide materials, as required in various applications.[15] Additionally, in relation to native GS T4P, the results are congruent with a previous study, which reported the enhancement of early bacterial attachment to Fe(III) oxide surfaces after denying a negatively charged post-translational tyrosine modification in the C-terminal region of GS pilin.[5]

Inspired by the ability of GS to reduce U ions via its T4P, we explored the interaction of the 20-mer peptide nanofibers with metal ions. Native GS T4P are associated with a c-type cytochrome,[16] implicated as the terminal reductase of a variety of metallic substrates owing to a low midpoint redox potential.[17] In the absence of cytochrome, we limited our investigation to the interaction with Au ions, which can be reduced by peptides,[18] do not precipitate or become reduced in phosphate buffer[19] that is required for the 20-mer self-assembly, and yield application-relevant reduced species.[20] $HAuCl_4$ was chosen as the ionic Au source due to the expected attraction of the $AuCl_4^-$ ion to the positively charged nanofibers.

Diluting preformed peptide nanofibers (1.66×10^{-3} M stock) to a volume fraction of 0.2 using aqueous $HAuCl_4$ and buffer (final concentrations of 1×10^{-3} and 9×10^{-3} M, respectively) led to sparse AuNP decoration of the nanofibers on a time scale of days at 25 °C (Figure S2, Supporting Information). The decoration process was significantly accelerated by overnight incubation of the mixture at 90 °C, a step which was adopted thereafter. High-resolution TEM-based methods confirmed the identity of the decorating particles as spherical AuNPs (Figure S3, Supporting Information). An increase in the degree of nanofiber decoration by AuNPs was achieved by decreasing the nanofiber volume fraction while maintaining the $HAuCl_4$ concentration fixed at 1×10^{-3} M. When the volume fraction was lowered from 0.2 to 0.015, the nanofiber floccule appeared to decrease in size and gain a darker color, and coloration of the liquid bulk was observed (**Figure 2**a). We focused on comparing the degree of nanofiber decoration in floccules from volume fractions of 0.2, 0.075, and 0.015. TEM analysis revealed that by lowering the nanofiber volume fraction, coverage of the nanofibers area by AuNPs increased remarkably from 22 ± 2% to 52 ± 3% and finally to 93 ± 1% at 0.2, 0.075, and 0.015 nanofiber volume fractions, respectively (Figure 2b,c). The AuNP coverage correlated well with the Au content as determined by thermogravimetric analysis (TGA), which showed a respective increase from 19% to 53% and finally to 88 wt% (Figure 2c and Figure S4, Supporting Information). Hence, these volume fraction conditions are denoted hereafter as sparse, moderate, and dense decoration, respectively. Further characterization, performed on the AuNPs following disintegration of the decorated nanofibers, showed that the AuNP size is larger and more heterogeneous at the dense decoration condition as compared with the other two conditions (Figure S5, Supporting Information). Taken

© 2019 WILEY-VCH Verlag GmbH & Co. KGaA, Weinheim

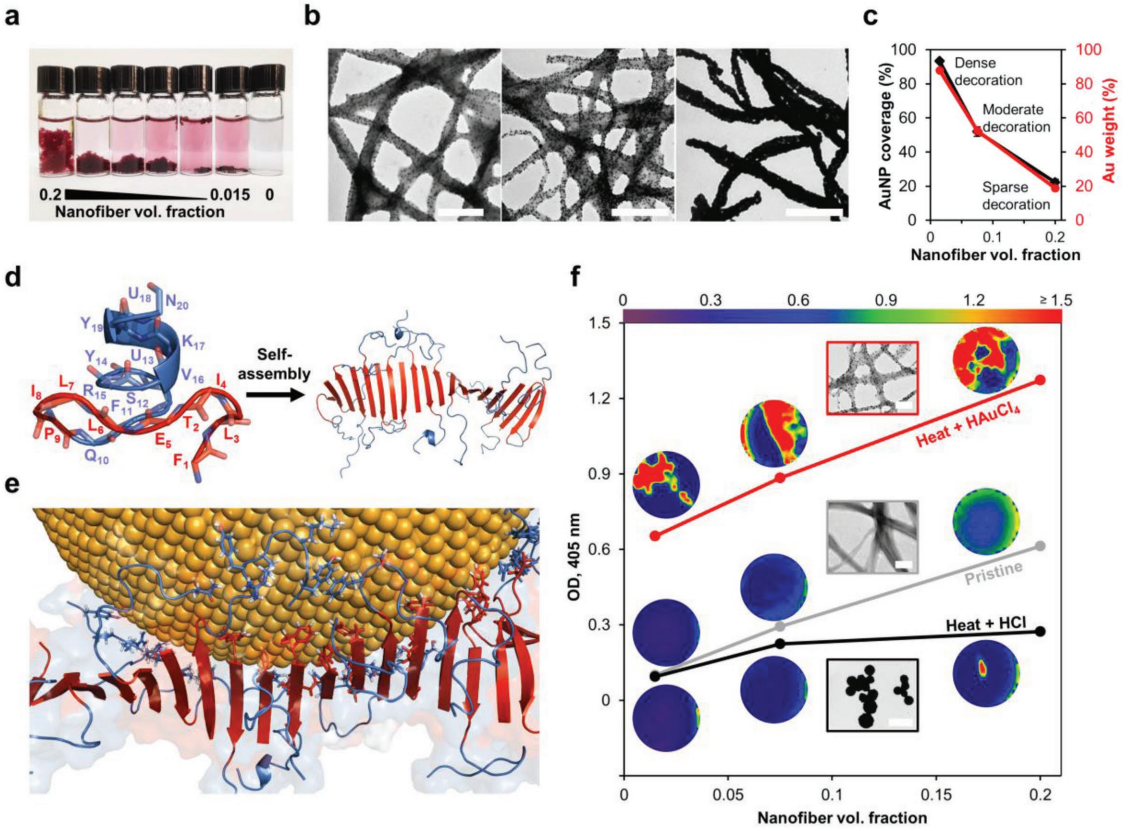

Figure 2. Formation of peptide–AuNPs nanocomposite. a) Photograph of peptide nanofibers and $HAuCl_4$ mixtures incubated at 90 °C. Rightmost vial is a similarly prepared control without peptide nanofibers. b) TEM images of AuNP-decorated nanofibers from 0.2, 0.075, and 0.015 volume fraction conditions (from left to right). Scale bars, 500 nm. c) TEM image analysis of single decorated nanofibers for estimating their coverage by AuNPs. Data represent mean ± standard error of the mean (n = 30 nanofibers per condition), for some data points the error bars are smaller than the symbol size. Au weight fraction, as determined by TGA, is shown for comparison. d) Lowest target function NMR structure of the 20-mer peptide, and a simplistic nanofiber model by MD simulation after 80 ns. NMR structure shows the peptide backbone as cartoon and sticks. Simulated model includes 20 peptide monomers, the backbones of which are shown as cartoon. P9 and the residues N-terminal to it are shown in red, residues C-terminal to P9 are shown in light blue. U denotes α-aminoisobutyric acid. e) Binding of a AuNP (10 nm diameter) to the nanofiber as modeled by MD simulation after 9 ns. All backbones are shown as cartoon and surface. Side chains of residues that strongly interact with the AuNP surface (d ≤ 4.5 Å) are shown as sticks. Color coding corresponds to the previous panel. f) Thermal stabilization of the peptide nanofibers by $HAuCl_4$ as evident by turbidometric area mapping. Plotted values are averages of turbidometric area maps at 405 nm. Color scale of the maps is defined in the top legend. Insets are corresponding TEM images from the 0.2 volume fraction condition. Frame colors of insets correspond to line colors. Scale bars: 200 nm for red and gray frames, 5 µm for black frame.

together, these results show that simple coincubation of the peptide nanofibers with $HAuCl_4$ at an elevated temperature yields a biometallic nanocomposite with a controllable degree of AuNP decoration to the extent of near-complete metallization.

Mechanistic insights into the process of AuNP decoration, i.e., ionic Au reduction and binding of the formed AuNPs, were obtained by combining analytical and spectroscopic methods, and molecular dynamics (MD) simulations. Tyrosine residues appear to participate in ionic Au reduction as dityrosine, an oxidation product of tyrosine,[21] was detected by high-performance liquid chromatography (HPLC) and liquid chromatography–mass spectrometry (LC–MS) analyses of decorated, but not pristine, nanofibers (Figure S6, Supporting Information). We note that although tyrosine is well known for its potent redox activity, other amino acids in the peptide may contribute to ionic Au reduction.[18] Next, the binding of AuNPs to the nanofibers was studied by spectroscopic methods and MD simulations. Using 2D NMR spectroscopy, we determined the solution structure of the 20-mer peptide in water (Figure 2d; for details see Section S1, Figures S7–S17, and Table S1, Supporting Information), which was overall consistent with its previous reductionist investigation.[8] This structure was utilized for constructing a simplistic nanofiber model in buffer, where residues N-terminal to the central proline residue (P9) are organized as a single supramolecular antiparallel β-sheet (Figure 2d, red), whereas the residues C-terminal to P9 flank the sheet and present partial helicity and high conformational flexibility (Figure 2d, light blue; for details see Section S2 and Figures S18 and S19, Supporting Information). AuNP binding was then investigated by simulating a single AuNP, modeled by a polarizable force field, in the proximity of the nanofiber for 9 ns. As shown in Figure 2e, multiple C-terminal regions interact with the AuNP, where mainly amine- or hydroxyl-bearing and aromatic residues form close contact with its surface (d ≤ 4.5 Å), in line with

© 2019 WILEY-VCH Verlag GmbH & Co. KGaA, Weinheim

their strong affinity to Au.[13,18] Considerably fewer N-terminal residues interacted thus with the AuNP surface, and the β-sheet hydrogen bonding network remained intact. These observations were supported experimentally by Fourier transform infrared (FTIR) spectroscopy (see Section S3, Figure S20, and Table S2, Supporting Information). C-terminal hook-like stretches therefore provide multiple anchoring points for binding the AuNP strongly to the nanofiber, the structure of which remains essentially unchanged in this process. Congruent with the latter conclusion is the observation that the decoration process structurally stabilizes the nanofibers. Turbidometric area mapping (Figure 2f) showed that nanofiber dispersions subjected to the decoration procedure present increased OD at 405 nm compared to dispersions of pristine nanofibers. In contrast, when $HAuCl_4$ is substituted in this procedure with HCl at an equivalent pH, the measured OD is lower than that of pristine nanofibers. These measurements suggest that pristine nanofibers may be impaired following incubation at 90 °C, unless supplemented by $HAuCl_4$. TEM imaging confirmed this assertion, showing that following incubation at 90 °C, $HAuCl_4$-treated nanofibers become decorated with AuNPs as described above, whereas HCl-treated nanofibers transform into coalescing spheres (Figure 2f). The interaction with $HAuCl_4$ therefore enhances the thermal stability of the nanofibers and prevents phase transition of the peptide.

In order to evaluate the potential applications of the peptide–AuNPs nanocomposite, we investigated its electronic, electrostatic, and surface adhesion properties. First, we investigated the electrical properties of individual AuNP-decorated nanofibers and their films. Single-fiber measurements were carried out using conductive-probe atomic force microscopy (CP-AFM), where current was measured along single nanofibers at varying distances from an evaporated top electrode. The calculated distance-normalized resistance was considerably lower for densely ($931 \pm 144\ \Omega\ \mu m^{-1}$) than for moderately ($1.46 \pm 0.82\ G\Omega\ \mu m^{-1}$) decorated nanofibers, and the former were also less sensitive to distance from the electrode, whereas sparsely decorated nanofibers exhibited very high resistance, within the instrumental noise level (**Figure 3**a). Next, the electrochemical transport characteristics of films cast from suspensions of the differently decorated nanofibers were measured in solution and under physiologically relevant range of temperatures using a bipotentiostat cyclic voltammetry configuration. Similar to the single-fiber measurements, films of densely decorated nanofibers presented the highest thickness-normalized conductance (445–427 S cm^{-1}) over a temperature range of 275–345 K, whereas sparsely decorated nanofiber films did not present appreciable conductance (Figure 3b). The measured increase in conductivity with decreasing temperature is consistent with metallic charge conduction through the AuNP network. Although the single fiber conductance values for moderately and densely decorated nanofibers differed by several orders of magnitude, bulk film conductivities differed by less than a factor of 2. The difference in relative conductances in the two measurement configurations may be attributed to the formation of a charge percolation network in the bulk film.[22] Taken together, these measurements indicate that the conductivity of individual nanofibers and nanofiber films increases with the density of Au decoration. Moreover, their conductivity also extends into the macroscale: AuNP-decorated nanofibers were fabricated into a 1.5 cm long film that enabled the activation of a serially connected light-emitting diode (LED, Figure 3c).

Electrostatic force microscopy (EFM) measurements were conducted on individual nanofibers from the three preparation conditions to explore their charge distribution and mobility properties. All decorated nanofibers responded to nonzero tip voltage due to buildup of static charge in the decorating AuNPs. We observed a parabolic phase response of the tip to applied voltage in the range ±5 V (Figure 3d), indicating attractive electrostatic force between the tip and the nanofibers, which scaled with the degree of decoration. It should be noted that while sparsely and moderately decorated nanofibers were measurable on a glass substrate, the densely decorated nanofibers strongly interacted with the tip to the extent that they detached from the glass surface during measurement. These nanofibers were measurable only when deposited on a conductive Au substrate, where the other nanofibers presented only negligible EFM signal due to weak coupling to the underlying substrate (Figure 3d; for details see Section S4 and Figure S21, Supporting Information). The symmetric tip response at both positive and negative tip bias indicated that all decorated nanofibers contain mobile charges, which attract the biased tip through image charge formation,[23] and are therefore highly polarizable.[24] As will be shown below, this property allowed for the construction of a static charge detector based on macroscopic deflection of the material.

We further characterized the densely decorated nanofibers due to their preferred electrical properties and higher Au content. We focused on their surface adhesion properties, which are of practical importance for utilization in applications. Dried nanofiber films were prepared on a range of substrate materials, which were subsequently immersed in water and subjected to rapid stirring. We observed that films on ceramic substrates (glass, titanium nitride, mica, and silicon) delaminated as a single cohesive patch within ≈10 s of immersion (Figure 3e and Movie S1, Supporting information). In contrast, films on polymeric, metallic, and modified glass substrates adhered and appeared undisturbed during the experimental timeframe, which was limited to 10 min (Figure 3e). Surface adhesion was further tested under more stringent conditions, where films on identical substrates were ultrasonicated in water for 5 min. Image analysis of pre- and post-treatment substrates showed the near-complete delamination of films from ceramic and two of the polymeric substrates, and their partial retention on the metallic and remaining polymeric substrates (Figure 3e). From this data, it is evident that densely decorated nanofibers can be utilized as either self-supporting immersible films or water-resistant coatings, owing to their substrate-selective adhesion. By casting the nanofiber dispersion into molds and allowing it to dry prior to immersion in water, we obtained cm-scale self-supporting immersed films of desired shapes (Figure 3f and Movie S2, Supporting Information). Scanning electron microscopy-based energy-dispersive X-ray spectroscopy (SEM-EDX) confirmed that both the AuNPs and peptide constituents are retained after water immersion (Figure 3f and Figure S22, Supporting Information) and confocal scanning laser microscopy (CSLM) revealed that such films are convex and reach ≈5 μm in thickness (Figure 3g).

© 2019 WILEY-VCH Verlag GmbH & Co. KGaA, Weinheim

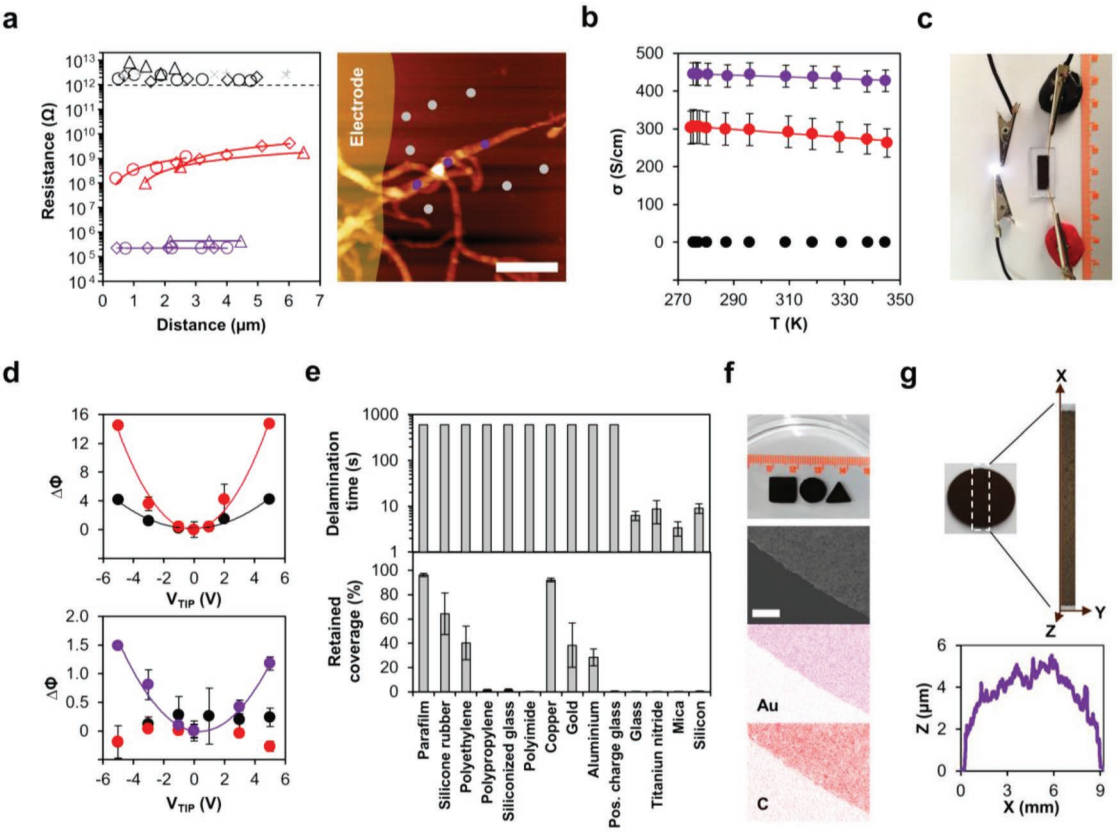

Figure 3. Physical properties of peptide–AuNPs nanocomposite. a) Left: CP-AFM measurements along single nanofibers from the sparse (black), moderate (red), and dense (purple) decoration conditions. Each symbol type represents measurements along a given nanofiber. Bare insulating surface adjacent to nanofibers (gray) was measured as control. Red and purple solid lines are linear fits. Dashed line represents the instrumental noise level. Right: Corresponding AFM image of densely decorated nanofibers. Purple and gray circles represent measurements along the nanofiber and on adjacent bare surface, respectively. Evaporated top electrode is false-colored yellow. Scale bar, 2 μm. b) Temperature-dependent conductivity of thickness-normalized nanofiber films from the sparse (black), moderate (red), and dense (purple) decoration conditions in 0.1 M phosphate–citrate buffer, pH 7.0. Solid lines are linear fits. Data represent mean ± standard error of the mean (see the Experimental Section in the Supporting Information for calculation). Horizontal and some of the vertical error bars are smaller than the symbol size. c) Photograph of a 1.5 cm long film of densely decorated nanofiber permitting the activation of a serially connected LED. d) EFM phase shift of single nanofibers from the sparse (black), moderate (red), and dense (purple) decoration conditions deposited on glass (top) or Au (bottom) surface. Densely decorated nanofibers were measurable only on the Au surface. Solid lines are quadratic fits. Data represent mean ± standard error of the mean ($n = 5$ measurements per nanofiber). e) Adhesion of densely decorated nanofiber films to various substrate materials in water, as estimated by delamination time during stirring (top) or retained coverage area following ultrasonication (bottom). Data represent mean ± standard error of the mean ($n = 5$ nanofiber-deposited substrates). f) Photograph of water-immersed self-supporting films of densely decorated nanofibers with shape side or diameter of 1 cm (top), and corresponding SEM-EDX image and elemental maps following transfer to a substrate and dehydration (bottom). Scale bar, 250 μm. g) Averaged thickness profile of densely decorated nanofiber films ($n = 3$ films), as measured by CSLM.

We utilized the densely decorated nanofiber films for three applications to demonstrate the multifunctionality of the T4P-inspired nanocomposite. First, the catalytic activity of the films was tested. A common model reaction for testing metal nanostructure catalysis was performed, where 4-nitrophenol is reduced to 4-aminophenol by $NaBH_4$ in the presence of a catalyst.[25] A circular nanofiber film coating was prepared on silicone rubber due to the adhesion of the nanofibers to this material, as shown in Figure 3e. When immersing the supported film in aqueous 4-nitrophenol with excess $NaBH_4$, a gradual decrease in absorbance at 400 nm and a concomitant increase in absorbance at 296 nm were observed (**Figure 4**a), as expected for the reaction.[25] The isosbestic points at 280 and 313 nm indicated that no by-products had formed.[26] Importantly, the extracted reaction rate constant ($k = 0.0082$ min^{-1}) remained nearly identical throughout four additional consecutive reaction cycles utilizing the same nanofiber coating (Figure 4a). Additionally, no catalytic activity was observed by bare silicone rubber (Figure S23, Supporting Information). Therefore, the peptide–AuNPs nanocomposite can function as a reusable catalytic coating. The substrate-selective adhesion and simple application onto a surface could allow for facile adaptation of the nanocomposite for various catalytic methodologies or processes. Thus, the T4P-inspired nanocomposite expands the scope of catalysis by metal-bearing supramolecular proteinaceous nanofibers, as introduced by others in recent years.[27]

Next, a static charge detector was prepared based on image charge attraction, as observed by EFM. To this end, a dry self-supporting film was fixed to a conductive element serially connected to an LED, and positioned such that it nearly

© 2019 WILEY-VCH Verlag GmbH & Co. KGaA, Weinheim

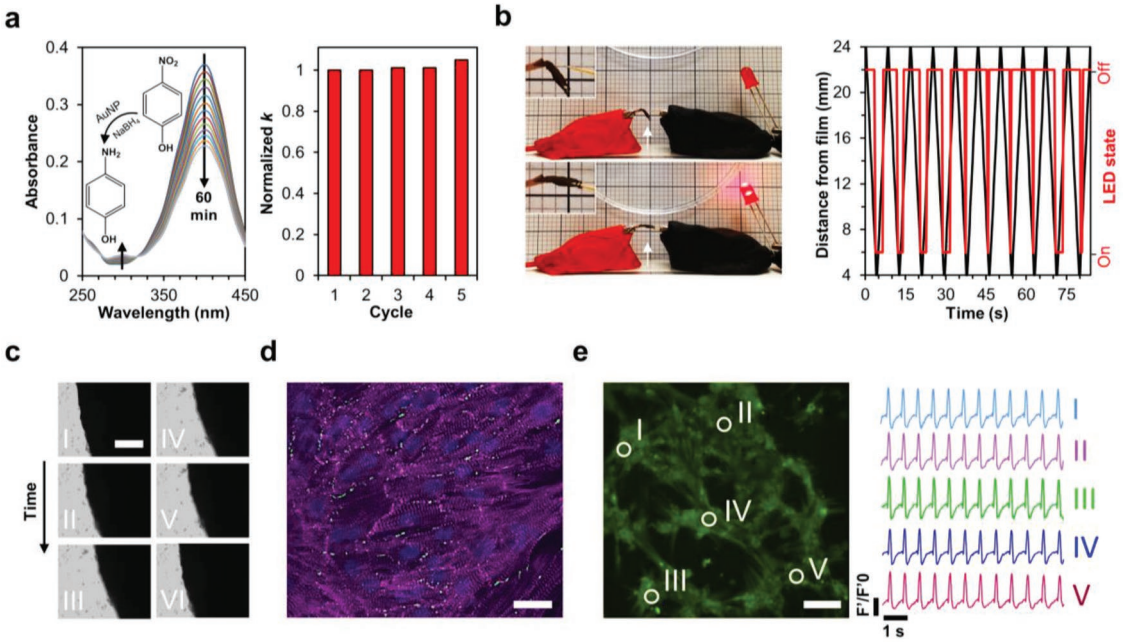

Figure 4. Applications of the peptide–AuNPs nanocomposite. a) Left: Time-dependent UV–vis spectra of the catalytic reduction of 4-nitrophenol to 4-aminophenol in the presence of nanofiber coating on silicone rubber surface. Inset is the reaction scheme. Right: Normalized rate constant for five consecutive reaction cycles using the same coated surface, demonstrating its reusability. b) Left: Photographs of a static charge detector based on nanofiber film deflection. The circuit is open and the LED is inactive when a statically charged polystyrene dish is far from the film (top). The film deflects to close the circuit, activating the LED, when the dish approaches the film (bottom). White arrows point to the film to guide the eye. Insets are magnified views of the film. Grid square side is 2 mm. Right: Time-dependent distance of the dish from the film (black) and corresponding LED state (red). During dish approach, the LED becomes activated at a distance of 6–7 mm. Data were calculated from Movie S3 in the Supporting Information. c) Optical microscopy image series of a circular nanofiber film cultured with cardiac cells after 5 days of incubation. The order of images is from top-left to bottom-right and the interval between images is 120 ms. The circle appears to contract (left column) and expand (right column), as also seen in Movie S4 in the Supporting Information. Scale bar, 250 µm. d) CSLM fluorescence image of immunostained cardiac α sarcomeric actinin (purple), connexin 43 (green), and nuclei (blue) in cardiac cells cultured on a circular nanofiber film. The image shows elongated and aligned cell bundles with massive striation. Scale bar, 25 µm. e) Left: Fluorescence microscopy image showing the regions of interest used for data quantification of calcium transient imaging. Scale bar, 50 µm. Right: Quantification of calcium transients by normalized fluorescence intensity over time, showing synchronized activity at the regions of interest. Data were calculated from Movie S5 in the Supporting Information.

contacted a second conductive element. A polystyrene dish, a statically-charged object under practical conditions,[28] was then set to approach the film periodically. At a consistent distance of 6–7 mm, the film deflected toward the dish, thereby transiently bridging the gap between the conductive elements and consequently permitting the LED activation (Figure 4b and Movie S3, Supporting Information). The film acted as a physical switch in this circuit owing to its attraction to static charge, conductivity, and flexibility. It should be noted that water-recovered films are generally brittle following dehydration, yet they presented sufficient flexibility and durability to enable device operation for at least tens of cycles.

Finally, due to their nanofibrous structure, conductivity, and immersibility, we were motivated to test the ability of the densely decorated nanofiber films to support the growth of electrogenic cells. Previously, it has been shown that cardiac cells benefit from nanostructured proteinaceous[29] and hybrid conductive[30] biomaterials. Therefore, cardiac cells were cultured on circular nanofiber films following their isolation from neonatal rats. After 5 days of incubation, the cells formed cell–cell interactions and assembled into functional cardiac films, exhibiting strong contraction forces (Figure 4c and Movie S4, Supporting Information). Development of these cardiac patches was then assessed by immunostaining for α-sarcomeric actinin, a protein associated with cell contraction, and connexin 43, which acts in electrical coupling between adjacent cells. As evident by α-actinin immunostaining (Figure 4d, purple), cardiac cells formed elongated and aligned cell bundles with massive striation, reminiscent of the natural cell morphology in the myocardium.[31] Furthermore, localization of connexin 43 between adjacent cardiomyocytes (Figure 4d, green) was in line with the observable contractions of the patches and suggested efficient electrical signal propagation between cells.[32] Indeed, calcium transient imaging confirmed that synchronized activation of cardiomyocytes occurred throughout the nanofiber films (Figure 4e and Movie S5, Supporting Information). The films therefore proved to be excellent biocompatible scaffolds, supporting the assembly of single cells into synchronized cardiac patches.

In summary, the current work presents for the first time the multifunctionality of the recently reported T4P-like peptide nanofibers. The bioinspired interaction of these designed self-assembled nanostructures with metal oxides or ions resulted in highly diverse nanocomposite materials. The interaction with Au ions is especially remarkable considering the exceptional degree of decoration by AuNPs, the simplicity of its

© 2019 WILEY-VCH Verlag GmbH & Co. KGaA, Weinheim

formation, and the lack of need to employ external additives such as reducing agents. The preferential formation of isotropic AuNPs over large anisotropic Au crystals is worth noting, as the latter were reported to form in recent studies utilizing amyloid nanofibers for elemental Au synthesis.[11,33] This dissimilarity may be explained by one or more crystallographic and redox chemistry mechanisms,[34] which are likely instigated by differences in sequence and localization of amino acids along the nanofiber. Such differences could facilitate binding of the nanofibers to a specific crystallographic face of Au nuclei and lead to their anisotropic growth, or alternatively enable nonspecific binding that results in isotropic growth and nanoparticle formation. In this context, we note that strongly reducing and binding cysteine residues as well as strongly complexing or reducing histidine or tryptophan residues[18] are absent in the T4P-like nanofibers but were present in amyloid nanofibers in the aforementioned studies. Moreover, the effect of amino acid identity and localization may be modulated by conformational flexibility of the nanofiber or regions thereof. Specifically, high conformational flexibility, as presented by the C-terminal stretches of the T4P-like nanofibers, is associated with increased binding affinity of peptides to the surface of AuNPs.[18] Further modulation could be exerted by higher-order organization of nanofibers into, e.g., a liquid crystalline nematic phase[33] or specific reaction conditions.[34]

The hybrid AuNPs–peptide material presented attractive functional properties that include electrical conductivity from the single-nanofiber level up and substrate-selective adhesion. The latter property allowed for the formation of macroscopic films that were either used as a coating or directly in their extremely thin free forms. The film preparation is notably simple, as it is based on a single-step green chemistry process followed by casting. The observed self-support and maintained integrity upon immersion are rarely observed in supramolecular peptide or protein-based materials, even after embedding inorganic materials or at increased film thickness. The absence of these properties typically precludes the use of such materials in various applications, whereas the presented hybrid AuNPs–peptide material was successfully utilized in several distinctly different applications. Looking forward, the hybrid material could be used for microelectronic circuit or sensor fabrication or be integrated with electroresponsive tissues for biomedical purposes.

Supporting Information

Supporting Information is available from the Wiley Online Library or from the author.

Acknowledgements

The authors acknowledge support from the Argentinean Friends of Tel Aviv University (T.G.), the European Research Council BISON project (grant agreement ID 694426), the Israeli National Nanotechnology Initiative, and Helmsley Charitable Trust (E.G.), the Air Force Office of Scientific Research Award No. FA9550-14-1-0350 and the U.S. Department of Education G.A.A.N.N fellowship (N.L.I. and A.I.H.), the Adams Fellowship Program of the Israel Academy of Sciences and Humanities (S.F.), the European Research Council Starting Grant No. 637943, the Slezak Foundation, and the Israeli Science Foundation (700/13) (T.D.), and the National Science Foundation (DMR-1506886) (P.K.). S.R. acknowledges joint research grant by DST, India through which 800 MHz NMR spectrometer was procured and used for NMR data collection. The authors thank George Levi (Tel Aviv University) for high-resolution TEM analysis and Diana Golodnitsky (Tel Aviv University) for TGA. T.G. thanks Zohar A. Arnon for his valuable assistance in figure preparation and additional members of the Gazit group for helpful discussions. Cardiac cells were isolated according to Tel Aviv University ethical use protocols L-14-040, 04-16-077.

Conflict of Interest

The authors declare no conflict of interest.

Keywords

biomaterials, biomimetics, hybrid materials, nanocomposites, peptide self-assembly

Received: November 9, 2018
Revised: December 20, 2018
Published online: January 15, 2019

[1] M. Georgiadou, V. Pelicic, in *Bacterial Pili: Structure, Synthesis and Role in Disease*, (Eds: M. A. Barocchi, J. L. Telford), CAB International, Wallingford, UK **2014**.
[2] G. Reguera, K. D. McCarthy, T. Mehta, J. S. Nicoll, M. T. Tuominen, D. R. Lovley, *Nature* **2005**, *435*, 1098.
[3] D. L. Cologgi, S. Lampa-Pastirk, A. M. Speers, S. D. Kelly, G. Reguera, *Proc. Natl. Acad. Sci. USA* **2011**, *108*, 15248.
[4] D. R. Lovley, *Curr. Opin. Electrochem.* **2017**, *4*, 190.
[5] L. V. Richter, A. E. Franks, R. M. Weis, S. J. Sandler, *J. Bacteriol.* **2017**, *199*, 1.
[6] a) L. Craig, N. Volkmann, A. S. Arvai, M. E. Pique, M. Yeager, E. H. Egelman, J. A. Tainer, *Mol. Cell* **2006**, *23*, 651; b) S. Kolappan, M. Coureuil, X. Yu, X. Nassif, E. H. Egelman, L. Craig, *Nat. Commun.* **2016**, *7*, 13015.
[7] T. Guterman, E. Gazit, *Bioelectron. Med.* **2018**, *1*, 131.
[8] T. Guterman, M. Kornreich, A. Stern, L. Adler-Abramovich, D. Porath, R. Beck, L. J. W. Shimon, E. Gazit, *Nat. Commun.* **2016**, *7*, 13482.
[9] a) R. Kirsch, M. Mertig, W. Pompe, R. Wahl, G. Sadowski, K. J. Böhm, E. Unger, *Thin Solid Films* **1997**, *305*, 248; b) T. Scheibel, R. Parthasarathy, G. Sawicki, X.-M. Lin, H. Jaeger, S. L. Lindquist, *Proc. Natl. Acad. Sci. USA* **2003**, *100*, 4527; c) F. Patolsky, Y. Weizmann, I. Willner, *Nat. Mater.* **2004**, *3*, 692; d) G. Wei, J. Reichert, K. D. Jandt, *Chem. Commun.* **2008**, *0*, 3903; e) G. Plascencia-Villa, J. M. Saniger, J. A. Ascencio, L. A. Palomares, O. T. Ramírez, *Biotechnol. Bioeng.* **2009**, *104*, 871; f) T. Yang, Y. Zhang, Z. Li, *Biomacromolecules* **2011**, *12*, 2027; g) G. Fang, Y. Yang, J. Yao, Z. Shao, X. Chen, *Mater. Sci. Eng., C* **2016**, *64*, 376.
[10] a) A. Orza, O. Soritau, L. Olenic, M. Diudea, A. Florea, D. Rus Ciuca, C. Mihu, D. Casciano, A. S. Biris, *ACS Nano* **2011**, *5*, 4490; b) S. Bolisetty, J. Adamcik, J. Heier, R. Mezzenga, *Adv. Funct. Mater.* **2012**, *22*, 3424; c) S. Bolisetty, R. Mezzenga, *Nat. Nanotechnol.* **2016**, *11*, 365; d) Y. Shen, L. Posavec, S. Bolisetty, F. M. Hilty, G. Nyström, J. Kohlbrecher, M. Hilbe, A. Rossi, J. Baumgartner, M. B. Zimmermann, R. Mezzenga, *Nat. Nanotechnol.* **2017**, *12*, 642.
[11] a) C. Li, S. Bolisetty, R. Mezzenga, *Adv. Mater.* **2013**, *25*, 3694; b) J. Zhou, A. Saha, J. Adamcik, H. Hu, Q. Kong, C. Li, R. Mezzenga,

 © 2019 WILEY-VCH Verlag GmbH & Co. KGaA, Weinheim

Adv. Mater. **2015**, *27*, 1945; c) G. Nyström, M. P. Fernández-Ronco, S. Bolisetty, M. Mazzotti, R. Mezzenga, *Adv. Mater.* **2016**, *28*, 472.
[12] a) I. A. Banerjee, L. Yu, H. Matsui, *Proc. Natl. Acad. Sci. USA* **2003**, *100*, 14678; b) M. Reches, E. Gazit, *Science* **2003**, *300*, 625; c) D. Gottlieb, S. A. Morin, S. Jin, R. T. Raines, *J. Mater. Chem.* **2008**, *18*, 3865; d) M. S. Lamm, N. Sharma, K. Rajagopal, F. L. Beyer, J. P. Schneider, D. J. Pochan, *Adv. Mater.* **2008**, *20*, 447; e) E. D. Sone, S. I. Stupp, *Chem. Mater.* **2011**, *23*, 2005; f) H. Ceylan, C. Ozgit-Akgun, T. S. Erkal, I. Donmez, R. Garifullin, A. B. Tekinay, H. Usta, N. Biyikli, M. O. Guler, *Sci. Rep.* **2013**, *3*, 2306.
[13] E. Kasotakis, E. Mossou, L. Adler-Abramovich, E. P. Mitchell, V. T. Forsyth, E. Gazit, A. Mitraki, *Biopolymers* **2009**, *92*, 164.
[14] a) C. Li, J. Adamcik, R. Mezzenga, *Nat. Nanotechnol.* **2012**, *7*, 421; b) M. Kosmulski, *J. Colloid Interface Sci.* **2014**, *426*, 209.
[15] a) E. Sharpe, R. Bradley, T. Frasco, D. Jayathilaka, A. Marsh, S. Andreescu, *Sens. Actuators, B* **2014**, *193*, 552; b) W. Song, D. Shi, S. Tao, Z. Li, Y. Wang, Y. Yu, J. Qiu, M. Ji, X. Wang, *J. Colloid Interface Sci.* **2016**, *481*, 100; c) W. Sun, J. Yang, J. Zhu, Y. Zhou, J. Li, X. Zhu, M. Shen, G. Zhang, X. Shi, *Biomater. Sci.* **2016**, *4*, 1422.
[16] C. Leang, X. Qian, T. Mester, D. R. Lovley, *Appl. Environ. Microbiol.* **2010**, *76*, 4080.
[17] X. Qian, T. Mester, L. Morgado, T. Arakawa, M. L. Sharma, K. Inoue, C. Joseph, C. A. Salgueiro, M. J. Maroney, D. R. Lovley, *Biochim. Biophys. Acta* **2011**, *1807*, 404.
[18] Y. N. Tan, J. Y. Lee, D. I. Wang, *J. Am. Chem. Soc.* **2010**, *132*, 5677.
[19] C. Engelbrekt, K. H. Sorensen, J. Zhang, A. C. Welinder, P. S. Jensen, J. Ulstrup, *J. Mater. Chem.* **2009**, *19*, 7839.
[20] S. Eustis, M. A. El-Sayed, *Chem. Soc. Rev.* **2006**, *35*, 209.
[21] S. Si, R. R. Bhattacharjee, A. Banerjee, T. K. Mandal, *Chem. - Eur. J.* **2006**, *12*, 1256.
[22] A. Heilmann, in *Polymer Films with Embedded Metal Nanoparticles*, (Eds: R. Hull, R. M. Osgood Jr., J. Parisi), Springer, New York **2003**.
[23] A. M. Stoneham, P. W. Tasker, *J. Phys. C: Solid State Phys.* **1985**, *18*, L543.
[24] a) D. D. Kulkarni, S. Kim, M. Chyasnavichyus, K. Hu, A. G. Fedorov, V. V. Tsukruk, *J. Am. Chem. Soc.* **2014**, *136*, 6546; b) O. Silberbush, M. Amit, S. Roy, N. Ashkenasy, *Adv. Funct. Mater.* **2017**, *27*, 1604624.
[25] T. Aditya, A. Pal, T. Pal, *Chem. Commun.* **2015**, *51*, 9410.
[26] Y. Mei, Y. Lu, F. Polzer, M. Ballauff, M. Drechsler, *Chem. Mater.* **2007**, *19*, 1062.
[27] a) C. M. Rufo, Y. S. Moroz, O. V. Moroz, J. Stöhr, T. A. Smith, X. Hu, W. F. DeGrado, I. V. Korendovych, *Nat. Chem.* **2014**, *6*, 303; b) S. Bolisetty, M. Arcari, J. Adamcik, R. Mezzenga, *Langmuir* **2015**, *31*, 13867.
[28] G. B. Gechele, G. Convalle, *J. Appl. Polym. Sci.* **1964**, *8*, 801.
[29] a) Y. Sun, Q. Jallerat, J. M. Szymanski, A. W. Feinberg, *Nat. Methods* **2014**, *12*, 134; b) A. K. Capulli, L. A. MacQueen, S. P. Sheehy, K. K. Parker, *Adv. Drug Delivery Rev.* **2016**, *96*, 83.
[30] a) T. Dvir, B. P. Timko, M. D. Brigham, S. R. Naik, S. S. Karajanagi, O. Levy, H. Jin, K. K. Parker, R. Langer, D. S. Kohane, *Nat. Nanotechnol.* **2011**, *6*, 720; b) S. Fleischer, M. Shevach, R. Feiner, T. Dvir, *Nanoscale* **2014**, *6*, 9410; c) M. Shevach, S. Fleischer, A. Shapira, T. Dvir, *Nano Lett.* **2014**, *14*, 5792.
[31] T. Dvir, B. P. Timko, D. S. Kohane, R. Langer, *Nat. Nanotechnol.* **2010**, *6*, 13.
[32] B. Weining, P. J. Christopher, B. Nenad, *Biofabrication* **2014**, *6*, 024109.
[33] S. Bolisetty, J. J. Vallooran, J. Adamcik, S. Handschin, F. Gramm, R. Mezzenga, *J. Colloid Interface Sci.* **2011**, *361*, 90.
[34] J. E. Millstone, S. J. Hurst, G. S. Métraux, J. I. Cutler, C. A. Mirkin, *Small* **2009**, *5*, 646.

© 2019 WILEY-VCH Verlag GmbH & Co. KGaA, Weinheim